euspen's 25th International Conference & Exhibition, Zaragoza, ES, June 2025
www.euspen.eu

Simultaneous nonlinear feedback and linear feedforward control design for high-performance motion control of machines for semiconductor manufacturing

Dragan Kostić[1], Luke F. van Eijk[1], Mojtaba Haghi[1], Wout Laarakkers[1], Jasper Gerritsen[1], Thom Samuels[1], Kai Wa Yan[1], Guido Knippels[1], Gary Widdowson[2]

[1]*ASMPT Limited, Center of Competency, The Netherlands*
[2]*ASMPT Limited, Hong Kong*

dragan.kostic@asmpt.com

Abstract
A simultaneous design of linear feedforward filters and nonlinear feedback controllers containing reset elements is explained in this contribution. The feedback reset controllers achieve higher controller bandwidths in comparison to conventional linear control strategies, which in turn enables better suppression of machine disturbances and vibrations induced by parasitic dynamics. The feedforward controller is a combination of components related to the reference position trajectory and its time-derivatives (e.g., velocity, acceleration, jerk, and/or snap). The obtained feedforward signal is then carefully filtered before being applied to the system, such as to minimize excitation of system resonances. Since too much filtering can also lead to degradation of motion tracking accuracy of the reference trajectory, a smart trade-off is made by means of the presented control design approach. Besides a mathematical formulation of the holistic design of nonlinear feedback and linear feedforward filters, the effectiveness of this contribution is demonstrated with an illustrative improvement of the motion performance of an ASMPT wire bonder machine. Measurement results obtained on this machine highlight the merits of the simultaneously designed nonlinear feedback and linear feedforward filters with respect to conventional (linear) feedback and feedforward control laws.

Reset control, feedforward filtering, high performance motion control, semiconductor industry, control design automation

1. Introduction

Ever-increasing performance and reliability requirements are posed on new generations of machines for semiconductor manufacturing. Products of ASMPT Ltd. are examples of such machines. Since fierce competition sets firm constraints on the market prices of these machines, advanced software motion control algorithms are preferable enhancers of machine capabilities compared to relatively expensive hardware solutions. In fact, advanced motion control is the critical enabler of high throughput, precision, and reliability of these machines. In this contribution we present a holistic approach to design feedback and feedforward laws for high-performance motion control. In particular, we explain the simultaneous design of linear feedforward filters and nonlinear feedback controllers containing reset elements. A concurrent design of feedback and feedforward controllers is proposed in [1]. However, that method is only applicable to preselected reference trajectories. Also, the feedback controllers are just linear ones.

In this contribution, we consider concurrent design of feedback and feedforward controllers that can accommodate a wide range of reference trajectories. Also, the feedback controllers are nonlinear and, thus, allow higher control bandwidths with respect to linear ones. We specifically use nonlinear reset control because of its well-developed frequency-domain design tools in comparison to other nonlinear control strategies [2]. We confine ourselves to single-input single-output (SISO) motion systems. In Figure 1, the dynamics of a SISO motion system are described in state-space with scalar input $u(t)$ and output $p(t)$, both functions of time t; SISO feedback and feedforward control laws are represented by u_{fb} and u_{ff}, respectively. The control design methodology to be described in this contribution can also be extended to systems with multiple inputs and outputs, but this is outside the scope of this paper.

In Section 2, we formulate the problem of simultaneous design of feedback and feedforward control laws. Section 3 describes a solution to this control problem including the mathematical description of a feedback reset controller. An industrial case-study of the simultaneous feedback and feedforward control design is shown in Section 4. Conclusions and an outlook of future developments are given in Section 5.

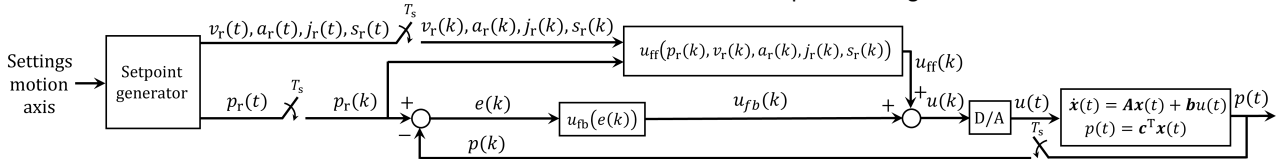

Figure 1. Generic control architecture of a SISO motion system.

2. Control problem formulation

A generic control architecture of a SISO motion system is depicted in Figure 1. Here, the reference position trajectory $p_r(t)$ is computed by a setpoint generator based on the desired motion distance, travel time, and constraints on time-derivatives of $p_r(t)$, such as the peak values of speed $v_r(t)$, acceleration $a_r(t)$, jerk $j_r(t)$, and snap $s_r(t)$; computation of the reference motion

profiles is explained in [3]. The reference motion profiles, denoted by subscript 'r', are computed using mathematical equations formulated in continuous time t. Position $p(t)$ of the controlled system is also in continuous time. However, due to digital control implementation, all time-variables are sampled at discrete-time $t_k = kT_s$, where T_s is the sampling period and $k \in \mathbb{N}_0$ denotes the sample number; for convenience, all sampled variables have k as argument. In Figure 1, position error e is defined as $e = p_r - p$, feedback control law u_{fb} is a function of e, feedforward control law u_{ff} is a function of the reference motion profiles, and total control signal $u = u_{fb} + u_{ff}$ is the input to the motion system, after being subject to digital-to-analog (D/A) conversion. Here, we assume linear-time invariant dynamics of the SISO motion system whose state-space model is given by $\dot{\boldsymbol{x}} = \boldsymbol{A}\boldsymbol{x} + \boldsymbol{b}u, p = \boldsymbol{c}^{\mathrm{T}}\boldsymbol{x}$, where $\boldsymbol{x}, \boldsymbol{b}, \boldsymbol{c} \in \mathbb{R}^l$, $\boldsymbol{A} \in \mathbb{R}^{l\times l}$, l denotes the number of states, and 'T' is the transpose operator.

In the business of development and engineering of semiconductor manufacturing equipment, there is an everlasting aspiration to achieve higher machine throughputs without increasing hardware costs. That requires optimization of all elements of the control system depicted in Figure 1. A method to optimize the reference trajectory is described in [3]. In the following section, we explain optimisation of the feedback and feedforward control laws u_{fb} and u_{ff}, respectively.

3. Simultaneous feedback and feedforward control design

Design and tuning of high-performance motion control algorithms, and especially full automation of these processes, are focal points of motion control teams at ASMPT. Instead of spending their own scarce time on controller design and tuning, the ASMPT control engineers are nowadays just focused on motion control performance specification, while the actual controller design and tuning is accomplished by control software. This sort of automation speeds up the design of high-performance motion control laws, enhances uniformity of controller tunings, reduces dependency on control experts, and raises interest of engineers without formal education in control technology to be involved in motion control.

The controller design and tuning of the controller settings is performed in the frequency domain using the loop-shaping method [4]. Here, we make use of sensitivity functions without and with the feedforward control law. Both sensitivity functions are formulated in the Z-domain [5]. The first one, S_{fb}, represents the transfer function from the reference position trajectory to the error with only the feedback control law included:

$$S_{fb}(z) = \frac{E(z)}{P_r(z)} = \frac{1}{1+P(z)C_{fb}(z)}, \tag{1}$$

where P_r and E represent the Z-transforms of $p_r(k)$ and $e(k)$, respectively, $C_{fb}(z)$ is a transfer function representation of the feedback control law u_{fb}, and $P(z)$ is a transfer function representation of the plant dynamics; here, $P(z)$ is the zero-order-hold (ZOH) discretisation [5] of the plant transfer function in the Laplace (s) domain $P(s) = \boldsymbol{c}^T(s\boldsymbol{I} - \boldsymbol{A})^{-1}\boldsymbol{b}$, where $\boldsymbol{I}$ is the $l \times l$ identity matrix. The second sensitivity function of concern, $S_{fb\&ff}$, represents the transfer function between the same variables as in (1) but now including the feedforward control law:

$$S_{fb\&ff}(z) = \frac{E(z)}{P_r(z)} = S_{fb}(z)\big(1 - P(z)C_{ff}(z)\big), \tag{2}$$

where $C_{ff}(z)$ is a transfer function representation of the feedforward control law u_{ff}.

Loop-shaping is performed on $S_{fb\&ff}$ while demanding that C_{fb} must stabilize the feedback control loop depicted in Figure 1 and imposing a stability robustness constraint on S_{fb}. In particular, the loop-shaping requirement is set by a frequency-dependent upper bound on the magnitude characteristics of $S_{fb\&ff}$:

$$|S_{fb\&ff}(f)| \le W_{fb\&ff}(f, f_1), \quad \forall f \le 0.5/T_s, \tag{3}$$

where f is a frequency in hertz, $0.5/T_s$ is the Nyquist frequency, $W_{fb\&ff} \in \mathbb{R}$ is a frequency-dependent upper bound on the magnitude of $S_{fb\&ff}$, and f_1 is the frequency where $W_{fb\&ff} = 1$. The bound $W_{fb\&ff}$ is specified by a control engineer as an array of data-points such as to cover all frequencies of interest for the desired performance of the motion control system considered. Since $W_{fb\&ff}$ is an array of data-points, $S_{fb\&ff}$ must be an array of data-points too; this is achieved by using the frequency response function (FRF) of the motion system, usually obtained by system identification, and by computing the frequency responses of C_{fb} and C_{ff} at the same frequency points as captured by the FRF of plant P.

Stability of the feedback control loop can be checked and verified with a data-driven method in the frequency domain, e.g. using the Nyquist stability criterion [4].

The stability robustness constraint is imposed as a frequency-dependent upper bound on the magnitude characteristics of S_{fb}:

$$|S_{fb}(f)| \le W_{fb}(f) \quad \forall f \le 0.5/T_s, \tag{4}$$

where W_{fb} is defined by a control engineer such as to ensure sufficient stability robustness of the feedback control loop depicted in Figure 1; a modulus margin of 2, which is a common stability robustness criterion, is achieved by imposing $W_{fb}(f) \le 2 \ \forall f \le 0.5/T_s$. Like $S_{fb\&ff}$, S_{fb} is represented by an array of data-points computed at the same frequencies as the FRF of P.

The specific frequency f_1 in (3) can be either specified by the control engineer or automatically tuned by the control software. In the former case, this frequency should be set such that a feasible set of controller parameters exists for which the closed-loop stability is guaranteed and the performance and robustness constraints in (3) and (4) can be satisfied. In the latter case, the algorithm for simultaneous tuning of C_{fb} and C_{ff} should aim at maximizing frequency f_1, while ensuring closed-loop stability and accommodating constraints (3) and (4).

In practice, C_{fb} and C_{ff} can be parameterized as discrete-time filters of desired orders. Below are the parametrizations considered at ASMPT:

$$C_{fb}(z) = \frac{U_{fb}(z)}{E(z)} = \frac{a_0+a_1z+\cdots+a_mz^m}{1+b_1z+\cdots+b_nz^n}. \tag{5}$$

$$C^*_{ff}(z) = \frac{U_{ff}(z)}{U^*_{ff}(z)} = \frac{c_0+c_1z+\cdots+c_pz^p}{1+d_1z+\cdots+d_qz^q}, \tag{6a}$$

$$u^*_{ff}(k) = \alpha_1 p_r(k) + \alpha_2 v_r(k) + \alpha_3 a_r(k) + \alpha_4 j_r(k) + \alpha_5 s_r(k), \tag{6b}$$

where $m \le n$ and $p \le q$ are the necessary conditions for realizability of the feedback and feedforward filters, respectively, $U_{fb}(z)$, $U_{ff}(z)$, and $U^*_{ff}(z)$ are the Z-transforms of $u_{fb}(k)$, $u_{ff}(k)$, and $u^*_{ff}(k)$, respectively, and u^*_{ff} is computed as a linear combination of components of the reference motion trajectory. Note that C_{ff} in (2) is a function of C^*_{ff} and u^*_{ff} defined by (6a) and (6b), respectively. Since according to (3) the loop-shaping is performed in the domain of frequencies in hertz, C_{ff} needs to be expressed in hertz too. That is done as follows:

$$C_{ff}(jf) = \frac{U_{ff}(jf)}{P_r(jf)} = \Big[\sum_{k=1}^{5} \alpha_k (j2\pi f)^{k-1}\Big] \cdot \Big[C^*_{ff}(z)\big|_{z=e^{j2\pi f T_s}}\Big], \tag{7}$$

where j is the unit imaginary number, such that $j^2 = -1$.

In (5) and (6), parameters $a_0,\ldots,a_m$, $b_1,\ldots,b_n$, $c_0,\ldots,c_p$, $d_1,\ldots,d_q$, and $\alpha_1,\ldots,\alpha_5$ are real-valued scalars that are simultaneously

tuned by the control software such as to accommodate constraints (3) and (4), ensure stability in the closed-loop, and even maximize the value of f_1. By maximizing f_1, we can achieve a broader frequency range where the position error e is attenuated with respect to the reference position trajectory p_{r}. Consequently, the control bandwidth of the control system depicted in Figure 1 is maximized.

In addition to a linear feedback filter (5), a nonlinear feedback control law can be engaged to improve trajectory tracking and settling control performance of the motion system. In particular, in this contribution we use a nonlinear resetting lag-filter, given in state-space representation by

$$R \coloneqq \begin{cases} \dot{x}_r(t) = -\omega_{r,\alpha} x_r(t) + \omega_{r,\alpha} e(t) & \text{if } e(t) \neq 0, \\ x_r(t^+) = 0 & \text{if } e(t) = 0, \\ y(t) = x_r(t), \end{cases} \tag{8}$$

with reset controller state $x_r \in \mathbb{R}$ and lag frequency $\omega_{r,\alpha} \in \mathbb{R}_{>0}$. If the input e is non-zero, the nonlinear filter behaves like a linear lag-filter. However, when the input is equal to zero, the reset element instantaneously resets the value of its state to zero. According to a describing function analysis (see [6] for details), a resetting lag-filter can achieve similar magnitude-characteristics as a linear lag-filter but with less phase lag. Therefore, as shown in [6], we can combine the resetting lag-filter with a linear lead-filter to obtain an element with a Constant Gain and Lead in Phase (CgLp), suggesting that we can break an inherent limitation of linear control: Bode's gain-phase relationship [6]. Namely, although the magnitude-characteristics of this CgLp-element are close to 1 in the entire frequency-range, we obtain a phase lead starting from frequency $\omega_{r,\alpha}$. To localize the nonlinearity only around the bandwidth frequency (to achieve more phase margin), we use a slightly modified version of the CgLp-element, as developed in [7]. Here, the linear lead-filter is replaced with a linear lead-lag filter, and a direct feed-through term (D_r) is added to the resetting lag-filter, such that it behaves like a resetting lag-lead filter. In this manner we still obtain a CgLp-element, but the phase lead only appears in a certain frequency-band (starting and ending at the lead and lag frequencies, respectively). With this 'free' phase margin we can increase error suppression in certain frequency ranges where vibrations are visible in the error when using the linear feedback controller. In the next section, we illustrate the data-driven controller synthesis method described above on an industrial use-case.

4. Industrial case-study

The simultaneous data-driven tuning of the feedback and feedforward controllers is illustrated on an ASMPT wire bonder. Figure 2 displays CAD drawings of this machine and its XYZ-motion platform. The wire-bonder makes movements at high speeds and accelerations to create, each second, multiple wired interconnections between a semiconductor die and its packaging. The XYZ-movements demand a precision of several micrometres. Right after each movement, bonding of the wire takes place for which a sub-micrometre position accuracy is required.

For confidentiality reasons, all data displayed in this section are normalized. In Figure 3, the magnitude and phase characteristics of the plant FRF are given in blue, representing the transfer from the input current to the driver of the motor actuating the X-axis of the wire bonder, to the position measured along this axis. The dashed black lines represent a rigid-body fit to the measured FRF data, which is attained by manual fitting of the speed and acceleration gains based on the magnitude plot of the plant FRF, together with a time-delay in the feedback loop which is fitted on the phase plot. The dashed red lines represent the inverse of the feedforward control law which is computed by automated fitting of a feedforward filter of the 2nd-order (6a) and coefficients α_2 and α_3 of the rigid-body part (speed + acceleration) of the feedforward function (6b), together with a time-delay; the automated fitting is performed using the software of ASMPT. By inspection of the plots shown in Figure 3, one can observe that the 'Rigid-body + 2nd-order filter fit' captures both the rigid-body dynamics of the plant (below normalized frequency $f \cong 10^{-1}$) and it over-fits the first resonance frequency (at normalized frequency $f = 0.144$). The reason for this over-fitting will be clarified later using Figure 5.

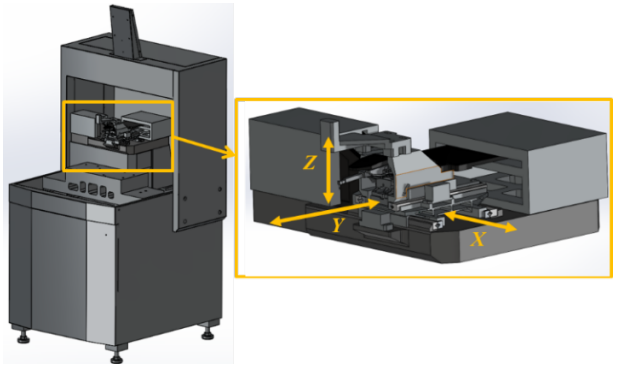

Figure 2. CAD drawing of an industrial wire bonder machine (on the left-hand side) and its XYZ-motion platform (on the right-hand side).

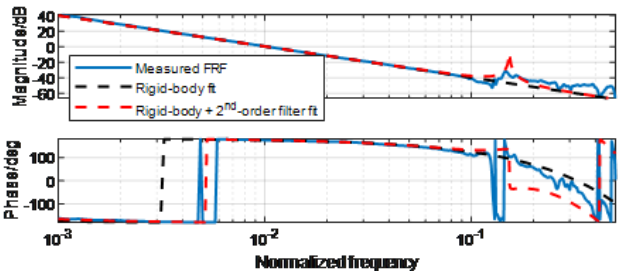

Figure 3. FRF measured on the X-axis of the wire-bonder and the parametric fits to be used for feedforward control.

In Figure 4 we show the magnitude characteristics of sensitivity function S_{fb} defined by (1), which incorporates the feedback controllers only. The blue plot represents S_{fb} computed based on the measured plant FRF (shown in Figure 3) and a linear feedback controller computed by automated tuning of a 6th-order filter (5) using the software of ASMPT. The horizontal dashed line represents the upper-bound W_{fb}, which imposes a limit of 6 dB on the peak magnitude of S_{fb}, which corresponds to a modulus margin of 2 (the stability robustness criterion). The red plot corresponds to S_{fb} computed using the same measured FRF and a nonlinear feedback controller; this controller contains the same 6th-order filter, but we add the CgLp-element and two additional 2nd-order filters. Each 2nd-order filter is targeted to decrease the sensitivity function in a certain frequency range, since the position errors achieved using the linear feedback controller have dominant energy in these two specific frequency bands. The sensitivity function S_{fb} with the nonlinear feedback is computed using the first-order describing function representation of the reset controller (see [6] for details). Its magnitude characteristics show better suppression of the position errors in two bands of the normalized frequencies: between $5{\cdot}10^{-3}$ and $1.1{\cdot}10^{-2}$ and between $1.7{\cdot}10^{-2}$ and $2.9{\cdot}10^{-2}$.

Magnitude plots of the sensitivity function $S_{\mathrm{fb\&ff}}$ defined by (2), which incorporates both the feedback and feedforward control laws, are shown in Figure 5. The blue plot corresponds to the case where the linear feedback controller (its $|S_{\mathrm{fb}}|$ is given by the blue plot in Figure 4) and the rigid-body feedforward control law (corresponding to the parametric fit given by the black dashed-line in Figure 3) are used. The red plot corresponds to

the use of the reset-control feedback (its $|S_{\mathrm{fb}}|$ is given by the red plot in Figure 4) and the 'Rigid-body + 2nd-order filter' feedforward (corresponding to the parametric fit given by the red dashed-line in Figure 3).

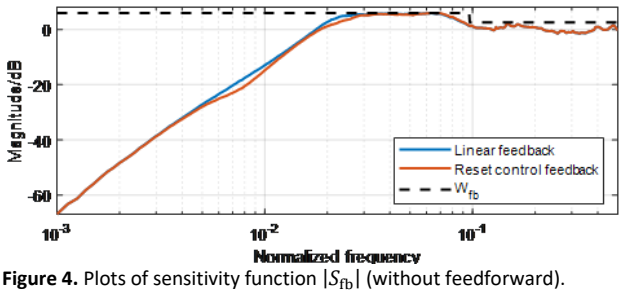

Figure 4. Plots of sensitivity function $|S_{\mathrm{fb}}|$ (without feedforward).

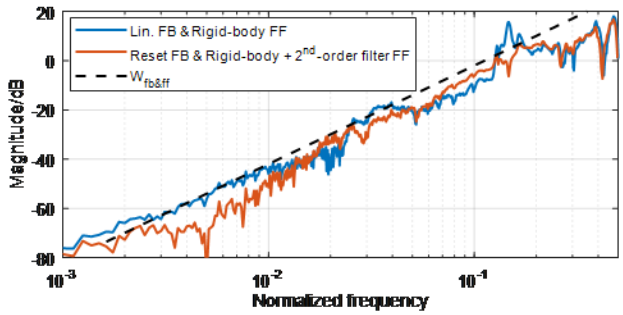

Figure 5. Plots of sensitivity function $|S_{\mathrm{fb\&ff}}|$ (with feedforward).

The dashed black line in Figure 5 represents the frequency-dependent upper bound $W_{\mathrm{fb\&ff}}$ on $|S_{\mathrm{fb\&ff}}|$ depicted in red colour. This bound is set by the control engineer and its frequency value f_1 is maximized by automatic tuning using the optimization software. To accommodate constraint (3) around the first resonance frequency of the plant (at a normalized frequency of 0.144), the 2nd-order feedforward filter over-fits this resonance, as observed in Figure 3. This increases performance robustness against this resonance in the control system depicted in Figure 1.

The two feedback & feedforward control designs are tested on the physical wire bonder machine in representative motion tasks that incorporate 6 motion distances (from short to long ones) performed in forward and backward directions (12 moves in total). The scaled reference position profiles are shown in black in Figure 6. The blue line represents the measured position error achieved using the linear feedback controller and the rigid-body feedforward. The red plot is the measured position error achieved using the feedback reset controller and the feedforward whose rigid-body part passes through the 2nd-order filter. The error plotted in red colour shows lower peak values than the error depicted in blue.

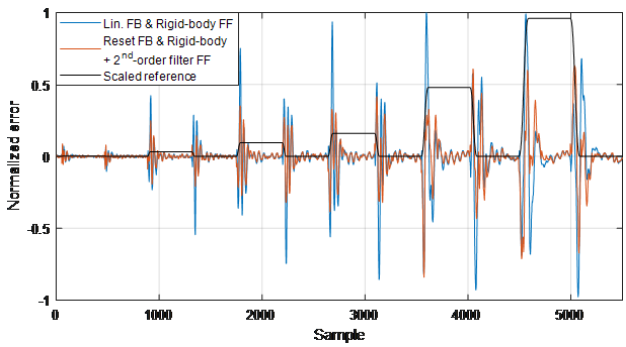

Figure 6. Measured position errors.

Better positioning accuracy using the simultaneously tuned nonlinear feedback and linear feedforward controller is verified by lower values of the root-mean-square (RMS) errors (normalized ones) displayed in Figure 7. Besides for the shortest motion distance (moves 1 and 2), for all other moves the reset controller with rigid-body and 2nd-order filter feedforward significantly outperforms application of the linear feedback and the rigid-body feedforward controllers. These improvements range from 5.5 % (move 2) up to even 56 % (move 4). This illustrates the effectiveness of the ASMPT optimization software for automated tuning of feedback and feedforward control laws.

Figure 7. RMS values of the measured position errors.

5. Conclusions and outlook

We developed a data-driven method for simultaneous tuning of nonlinear feedback reset controllers and linear feedforward filters. This method utilizes the loop-shaping control design in the frequency domain. Inputs of this methodology are the plant frequency response data obtained by system identification, the desired parameterisations of the feedback and feedforward control laws, and frequency-dependent bounds on the magnitude characteristics of the sensitivity functions, representing the transfer functions from the reference position trajectory to position error, without and with feedforward control laws incorporated. The outputs are automatically and optimally tuned feedback and feedforward controller settings. This framework is practically demonstrated by simultaneous tuning of feedback and feed-forward controllers for a motion axis of an ASMPT wire bonder machine. The resulting controllers outperform conventional linear motion controllers in representative motion tasks up to even 56 % in terms of root-mean-square error values. In the future, this framework will be extended to simultaneous tuning of feedback and feedforward control laws for systems with multiple inputs and outputs. Also, attention will be given to speeding up the optimisation algorithm.

References

[1] Peng C and Tomizuka M 2018 Concurrent Design of Feedforward and Feedback Controller for Building Thermal System *Proc. IEEE Conf. Decis. Control* 5257–63

[2] Caporale D, van Eijk L F, Karbasizadeh N, Beer S, Kostić D and HosseinNia S H 2024 Practical Implementation of a Reset Controller to Improve Performance of an Industrial Motion Stage *IEEE Trans. Control Syst. Technol.* **32(4)** 1451-62

[3] Kostić D, Tsai Y R, Tsai Y L, Haghi M, Gerritsen J, Yan K W, Laarakkers W and Knippels G 2024 Multi-objective reference trajectory optimisation for improved accuracy and throughput of high-tech mechatronics motion systems *Proc. EUSPEN SIC Precision Motion Systems & Control,* 's-Hertogenbosch, The Netherlands

[4] Åström K J and Murray R M 2009 *Feedback Systems: An Introduction for Scientists and Engineers* (Princeton Univ. Press)

[5] Franklin G F, Powell J D and Workman M L 1997 *Digital Control of Dynamic Systems* (Ellis-Kagle Press)

[6] Saikumar N, Sinha R K and HosseinNia S H 2019 "Constant in Gain Lead in Phase" Element– Application in Precision Motion Control *IEEE/ASME Trans. Mechatron.* **24(3)** 1176-85

[7] Quinten F 2024 *Closed-loop frequency domain reset control design, application on an industrial motion platform* MSc thesis, Report No 2024.104 (Delft University of Technology)